Author(s): Shakespeare, Cliona; Loippo, Teemu; Lyyra, Henri; Muhonen, Juha T.

Title: The effects of ion implantation damage to photonic crystal optomechanical resonators in silicon

Year: 2021

Version: Published version

Shakespeare, C., Loippo, T., Lyyra, H., & Muhonen, J. T. (2021). The effects of ion implantation damage to photonic crystal optomechanical resonators in silicon. Materials for Quantum Technology, 1(4), Article 045003. https://doi.org/10.1088/2633-4356/ac3e42

The effects of ion implantation damage to photonic crystal optomechanical resonators in silicon

Materials for Quantum Technology

PAPER

The effects of ion implantation damage to photonic crystal optomechanical resonators in silicon

Cliona Shakespeare, Teemu Loippo, Henri Lyyra and Juha T Muhonen*

Department of Physics and Nanoscience Center, University of Jyväskylä, PO Box 35, FI-40014 University of Jyväskylä, Finland
* Author to whom any correspondence should be addressed.

E-mail: juha.t.muhonen@jyu.fi

Keywords: photonic crystal, ion implantation, optomechanics, silicon, nanomechanical resonator

Supplementary material for this article is available online

OPEN ACCESS

RECEIVED
12 October 2021

REVISED
22 November 2021

ACCEPTED FOR PUBLICATION
29 November 2021

PUBLISHED
17 December 2021

Abstract

Optomechanical resonators were fabricated on a silicon-on-insulator substrate that had been implanted with phosphorus donors. The resonators' mechanical and optical properties were then measured (at 6 K and room temperature) before and after the substrate was annealed. All measured resonators survived the annealing and their mechanical linewidths decreased while their optical and mechanical frequencies increased. This is consistent with crystal lattice damage from the ion implantation causing the optical and mechanical properties to degrade and then subsequently being repaired by the annealing. We explain these effects qualitatively with changes in the silicon crystal lattice structure. We also report on some unexplained features in the pre-anneal samples. In addition, we report partial fabrication of optomechanical resonators with neon ion milling.

1. Introduction

Ion implantation is a widely-used technology for doping of semiconductors with applications varying from microchips [1, 2], to solar panels [3], to quantum computing [4]. As ion implantation is a somewhat destructive method, basically bombarding the substrate with high-energy ions, the process inevitably damages the crystal structure of the substrate. This problem is especially acute with silicon, as it is easily damaged and can become amorphous [5].

The implantation damage is usually healed with a post-implantation anneal [6] that both allows the crystal to repair itself and activates any substitutional donor atoms as they can then take their place in the crystal structure. Here we study the effects of the implantation damage and subsequent annealing to the mechanical and optical properties of suspended photonic crystal nanobeams.

The degradation of the mechanical properties of the suspended silicon structures we observe will be of importance to any studies combining implanted ions and mechanical systems (such as hybrid structures combining donor spin qubits [7, 8] with phonon buses [9]). The changes in the optical properties might be of importance to any devices combining ion implantation and photonic crystals in silicon, a field that is expected to grow in importance as single-photon emitters in silicon are being actively investigated [10–13].

2. Structures

The resonators we study, as shown in figure 1, are sliced photonic crystal nanobeams, the general design of which was presented in reference [14] and similar structures were also used in later studies [15, 16]. Details of the exact design studied here are shown in the supplementary material [17]. The photonic crystal pattern in the centre of the nanobeam supports different optical modes than the photonic crystals on the sides, which work as Bragg reflectors for the targeted cavity mode. Note that here we do not have a tapering region between the mirrors and the cavity, although it has been shown to decrease the optical linewidth considerably [15]. The cavity optical mode has an electric field maximum at the centre of the silicon beam. The small vacuum gap

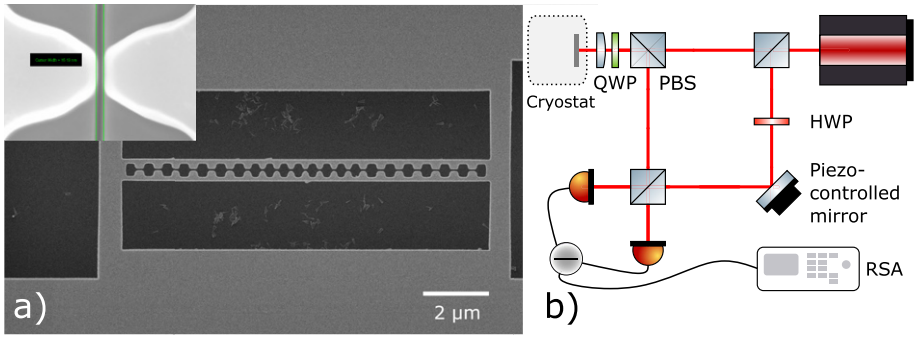

Figure 1. (a) HIM image of a nanobeam with same design as the ones studied here (from the same chip). Grey parts are free hanging silicon and the dark parts show the substrate 3 μm below. The optical cavity is located at the centre of the silicon nanobeam where the photonic crystal lattice constant is smaller. The two beam halves have been separated by a small gap. Inset: a SEM image of the gap between nanobeam teeth showing the roughly 20 nm separation before suspension that was defined with neon ion milling. (b) Schematic of the interferometer used for measurements; QWP refers to a quarter-wave-plate, HWP to a half-wave-plate, PBS to a polarizing beam splitter and RSA to a realtime spectrum analyzer.

between the two beam halves leads to strong field confinement in the gap, and a large frequency dependence of the optical mode on the gap size. This gives strong optomechanical coupling for the mechanical mode where the two beam halves move asymmetrically in-plane (breathing mode).

The samples were fabricated on a silicon-on-insulator wafer with 220 nm device layer and 3 μm buried oxide. The device layer was implanted with phosphorus ions. The ion implantation [18] aimed for a constant donor density of 10^{17} ions cm^{-3} in the device layer and was done in three steps: 110 keV energy with a dose of 1.5×10^{12} ions cm^{-2}, 40 keV with 5×10^{11} ions cm^{-2} and 20 keV with 1.5×10^{11} ions cm^{-2}. The wafer was not annealed after implantation, leaving any potential lattice damage intact.

The wafer was then diced and optomechanical resonators were fabricated on chips. The chips were spin coated first with Microchem 950 k PMMA A4 resist, which was then baked for 3 min on a hotplate at 160°C, then with Allresist AR-PC 5090.02 (Electra 92), which was baked for 1 min at 80°C on a hotplate. The resist was patterned with a Raith eLine electron beam lithography tool. The PMMA was developed for 20 s in a 2:1 mixture of IPA and MIBK. Before development, the Electra 92 resist was washed off. The etching was done with an Oxford Plasmalab 80 reactive ion etcher with 80 sccm SF_6 and 20 sccm O_2 at 30 mTorr at −100°C using liquid nitrogen cooling.

The gap between the beam halves was afterward milled through with 28 keV neon ions in a Zeiss Orion NanoFab helium ion microscope (HIM). Simulations of the neon milling with SRIM [19] (28 keV ion energy, 3–4 pA ion current, 7.5 nC μm^{-2} area dose) show a lateral ion path of up to 30 nm, so there should be only a moderate amount of neon ions in the silicon nanobeams from the milling. Finally the optomechanical structures were released by wet etching the oxide layer with 48% HF for 4 min. An example of a released structure is shown in figure 1(a).

A picture of the milled gap between the beam halves is shown in the inset of figure 1(a) where the high resolution enabled by neon milling is demonstrated as the gap is only 20 nm wide. This would be beneficial for optomechanical applications as the optomechanical coupling strength in these devices grows with decreasing gap size. However, scanning electron micrograph (SEM) images taken after the HF release show an opening of roughly 50 nm. This could be due to the beam halves bending outwards from stress or charging but requires further study.

3. Measurements

The samples were placed inside a Montana instruments C2 s50 cryostat and measured with a balanced homodyne interferometer (schematic in figure 1(b)) using near infrared wavelengths. The optical cavity was coupled into from above with a free space laser beam and the reflected light was interfered with a reference laser beam. The interference signal as a function of laser wavelength was measured with a subtracting detector and a spectrum analyzer. Lorentzian line shapes were fitted to the brightest mechanical peak visible in each spectrum (using the Python package SciPy [20]) and the optical and mechanical resonance frequencies and linewidths were extracted from these fits. As we do not lock the phase of the interferometer but average over all the phases by sweeping a piezo mirror in the local oscillator arm, our mechanical peaks split with the frequency of the a sweep (c. 100 Hz). The effective optical linewidth is also modified. We account for both of these effects in our fitting procedures.

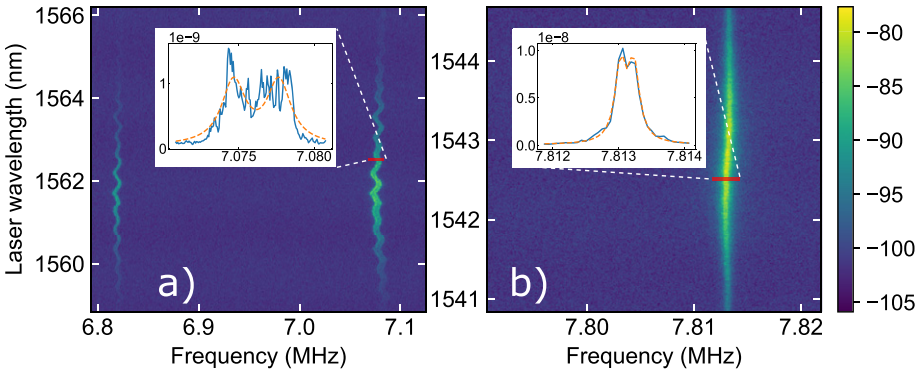

Figure 2. Resonator 2 spectrogram measured at 6 K before (a) and after (b) annealing as a function of the laser wavelength. The colorbar shows the power of the interferometer signal in dB. Crosscuts of the spectra (on a linear scale) are shown in the insets with Lorentzian fits (dashed line). The post-anneal sample exhibits much clearer Lorentzian resonance. The pre-anneal sample has two unexpected features: the oscillation of the resonance frequency and the splitting of the mode into two separate peaks separated by few kHz. Note that the small splitting in the post-anneal sample (by 100 Hz) is caused by the phase averaging in the measurement (see text). In the pre-anneal sample there is another mechanical mode visible at around 6.8 MHz which also shows the oscillations.

After measuring the resonators at both room temperature and 6 K, the samples were taken out and annealed in a tube furnace for 30 min at 600°C and 15 s at 1000°C, after which they were put to 500°C for 5 min before taken out of the oven. The last step was included for a gentler cool down process. All annealing was done in an argon atmosphere with 1 atm pressure. The chip was left to cool overnight, after which the chip was loaded into the cryostat and the measurements at room temperature and 6 K repeated.

4. Results and discussion

All data presented has been measured from two different resonators on the same chip, which we name resonator 1 and resonator 2. They are nominally identical in design, except that resonator 2 has been scaled in two dimensions by a factor of 1.04 compared to resonator 1. (The thickness is defined by the substrate and cannot be scaled.) We note that the differences we observe between the two samples stem mainly from fabrication imperfections [17] as we elaborate below.

The wavelength dependent spectrogram of the interferometer signal from resonator 2 is shown in figure 2. Similar data from resonator 1 is shown in the supplementary material [17]. The thermally driven mechanical vibrations are visible in the interferometer signal when the laser wavelength is close to the optical cavity resonance frequency. An unexpected phenomenon was the oscillation of the mechanical resonance frequency as a function of the laser wavelength in the pre-anneal samples at 6 K, as shown in figure 2(a). This effect was present in both resonators though much more noticeable in resonator 2 and disappeared after annealing. The oscillation was consistent between consecutive measurements (meaning the same wavelength would produce same response) but varied when the laser spot position (with regards to the silicon nanobeam) was moved. Changing the laser power by a factor of 5 had no significant effect on the phenomenon, implying it is not a thermal effect. Also, the mechanical resonances in the pre-anneal samples seemed to occasionally split to two modes separated by a few kHz but this varied with both laser wavelength and time. This splitting was visible only at 6 K temperatures. When extracting the parameters below, we fit this data assuming two modes.

After annealing the mechanical resonance frequencies increased consistently by ∼10% for both samples at both temperatures, as pictured in figure 3, with pre-anneal frequencies lying in the range of 7–8 MHz. An increase in resonance frequency implies a stiffer resonator, i.e., a higher Young's modulus. The Young's modulus for silicon depends on crystal orientation [21] and is higher for crystalline silicon in the fabrication direction of our device (166 GPa for crystal direction [110]) than for polycrystalline silicon (155 GPa). This means that the shift in resonance frequency can at least qualitatively be explained by the lattice structure being damaged by the ion implantation—making it in effect more polycrystalline-like—and then being reconstructed by the annealing.

To study the effect further, we made COMSOL simulations of the beams' mechanical resonance frequencies using both polycrystalline silicon and single-crystalline silicon with the same crystal direction as our sample. The details of the COMSOL simulation are presented in the supplementary material [17]. The simulated resonance frequencies for resonator 1 were 6.6 MHz for polycrystalline silicon and 6.8 MHz for single-crystalline silicon. For resonator 2 the values were 6.4 MHz and 6.6 MHz, respectively. This is in qualitative agreement with the measurements but the measured shifts are consistently higher than this effect alone would predict.

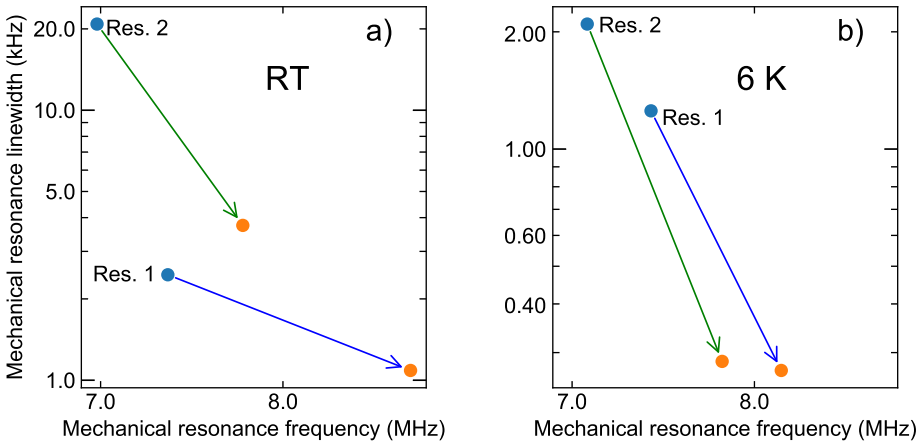

Figure 3. Plots of the resonators' mechanical resonance frequencies and linewidths before (blue) and after (orange) the annealing at room temperature (a) and 6 K (b). The values before and after annealing have been connected with blue (resonator 1) and green (resonator 2) arrows for clarity.

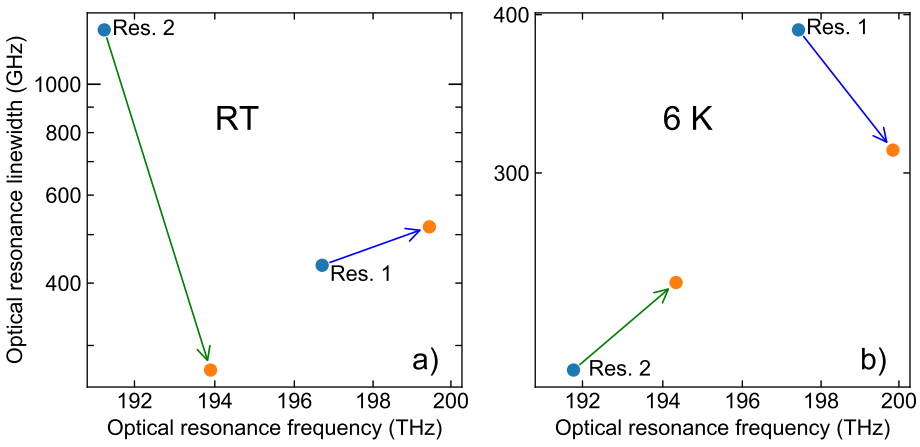

Figure 4. Plots of the resonators' optical resonance frequencies and linewidths before (blue) and after (orange) the annealing at room temperature (a) and 6 K (b). The values before and after annealing have been connected with blue (resonator 1) and green (resonator 2) arrows for clarity.

The mechanical linewidths for both resonators decreased after the anneal. Interestingly all measured modes (including unshown less bright modes) ended up with a linewidth of 0.2–0.3 kHz at cryogenic temperatures after the anneal, possibly indicating a limit where some mechanism not related to temperature or crystal damage is determining the linewidth (such as clamping losses). In room temperature measurements resonator 1's linewidth improved by a factor of 2 whereas resonator 2 had an improvement by factor of 6. The trend is consistent with the lattice structure healing from implantation damage during the annealing, as lattice defects can cause mechanical damping [22].

We note that the changes in the mechanical frequencies and linewidths between room temperature and 6 K are a known feature with these kinds of structures and are presumably related to the stress/strain of the samples changing during the cooldown (due to the mismatch in thermal expansion between the silicon device layer and the underlying silicon dioxide).

The changes in the optical properties during annealing are presented in figure 4. The optical cavity resonance frequency and cavity linewidth can be extracted from the strength of the optomechanical signal as a function of the laser wavelength. The optical resonance frequencies increased by ∼1% during the anneal. Here there are two effects that might be playing a role: (i) a decrease in the effective refractive index or (ii) change in the equilibrium gap size between the beams due to mechanical reasons. We unfortunately cannot completely untangle these effects. The refractive index of polycrystalline silicon is higher than that of single-crystal silicon [23]. Thus recrystallization of the silicon lattice could lead to a lowering of refractive index and a resonance shift toward higher optical frequencies in accordance with our results. We also imaged the sample with SEM before and after annealing and saw no visible change in the gap size. Note that the doping concentration should not affect the effective refractive index at these wavelengths and doping levels [24].

For the optical linewidth we did not recover any consistent trend. We note that there could be two competing factors here. Silicon crystal lattice damage can be expected to cause photon losses to increase, and polycrystalline silicon also has a higher coefficient of absorption at these wavelengths [25], which means that annealing should decrease the linewidth. On the other hand, doping activation during annealing would be expected to cause photon losses to increase.

We presume that the fact that there is a considerable difference between the two resonators in their optical properties (before and after annealing) is due to fabrication imperfections. The fabrication procedure for the samples here is somewhat non-conventional as we did not use an ICP-RIE (but a regular RIE) and we milled the gap between the two beams with neon milling. The relatively large differences in the optical quality are most likely explained by the neon milling which required drawing the milling line 'by hand' when looking at the neon ion image, so the alignment accuracy is poor. There are also some charging effects in play that cause variations in the milling. Overall, this is still a very experimental way to fabricate these devices and leads to large variability in the parameters.

5. Conclusions

In conclusion, we have shown that post-implantation annealing has a significant effect on the optical and especially the mechanical properties of silicon photonic crystal nanobeams. The exact mechanisms of the effects we demonstrated still require further study but can qualitatively be explained by implantation damage making the silicon more polycrystalline-like and annealing then recovering the single-crystalline structure. These findings will have relevance to any nanophotonic device that combines ion implantation with photonic crystal structures, particularly the emerging field of spin-photonics in silicon as well as to any structures combining ion implantation and mechanical devices in silicon. The pre-anneal samples exhibited several unexplained features that could bear further investigation.

Acknowledgments

We acknowledge Luke Antwis and Roger Webb for help with the ion beam implantations. This project has received funding from the European Research Council (ERC) under the European Union's Horizon 2020 research and innovation programme (Grant Agreement No. 852428), from Academy of Finland Grant No. 321416 and Jenny and Antti Wihuri Foundation.

Data availability

The data that support the findings of this study are available upon reasonable request from the authors.

ORCID iDs

Cliona Shakespeare https://orcid.org/0000-0002-3654-2229
Teemu Loippo https://orcid.org/0000-0001-7545-0936
Henri Lyyra https://orcid.org/0000-0002-9218-4657
Juha T Muhonen https://orcid.org/0000-0001-6520-6999

References

[1] Poate J M and Saadatmand K 2002 *Rev. Sci. Instrum.* **73** 868–72
[2] Rubin L and Poate J 2003 *Ind. Phys.* **9** 12 https://web.archive.org/web/20071011192314/http://aip.org/tip/INPHFA/vol-9/iss-3/p12.html
[3] Rohatgi A, Meier D L, McPherson B, Ok Y-W, Upadhyaya A D, Lai J-H and Zimbardi F 2012 *Energy Procedia* **15** 10–9
[4] van Donkelaar J *et al* 2015 *J. Phys.: Condens. Matter.* **27** 154204
[5] Williams J S 1998 *Mater. Sci. Eng.* A **253** 8–15
[6] Ziegler J F 1985 *Nucl. Instrum. Methods Phys. Res.* B **6** 270–82
[7] Pla J J, Tan K Y, Dehollain J P, Lim W H, Morton J J L, Jamieson D N, Dzurak A S and Morello A 2012 *Nature* **489** 541–5
[8] Muhonen J T *et al* 2014 *Nat. Nanotechnol.* **9** 986–91
[9] Patel R N, Wang Z, Jiang W, Sarabalis C J, Hill J T and Safavi-Naeini A H 2018 *Phys. Rev. Lett.* **121** 040501
[10] Chen S, Raha M, Phenicie C M, Ourari S and Thompson J D 2020 *Science* **370** 592–5
[11] Bergeron L *et al* 2020 *PRX Quantum* **1** 020301
[12] Weiss L, Gritsch A, Merkel B and Reiserer A 2021 *Optica* **8** 40–1
[13] Durand A *et al* 2021 *Phys. Rev. Lett.* **126** 083602

[14] Leijssen R and Verhagen E 2015 *Sci. Rep.* **5** 15974
[15] Leijssen R, La Gala G R, Freisem L, Muhonen J T and Verhagen E 2017 *Nat. Commun.* **8** ncomms16024
[16] Muhonen J T, La Gala G R, Leijssen R and Verhagen E 2019 *Phys. Rev. Lett.* **123** 113601
[17] See supplemental material at (https://stacks.iop.org/MQT/1/045003/mmedia)
[18] Implantation was carried out in the ion beam centre of University of Surrey.
[19] Ziegler J F, Ziegler M D and Biersack J P 2010 *Nucl. Instrum. Methods Phys. Res.* B **268** 1818–23
[20] Virtanen P *et al* (SciPy 1.0 Contributors) 2020 *Nat. Methods* **17** 261–72
[21] Hopcroft M A, Nix W D and Kenny T W 2010 *J. Microelectromech. Syst.* **19** 229–38
[22] Shin J, Choi K, Shiko S, Choi H and Bae D 2015 *Composites* B **77** 194–8
[23] Jones R E and Wesolowski S P 1984 *J. Appl. Phys.* **56** 1701–6
[24] Auslender M and Hava S 2017 *Single-Crystal Silicon: Electrical and Optical Properties* (Berlin: Springer)
[25] Harbeke G, Krausbauer L, Steigmeier E F, Widmer A E, Kappert H F and Neugebauer G 1984 *J. Electrochem. Soc.* **131** 675–82